CHAPTER IV. DOPED METAL OXIDE SYSTEMS

IV.1-- INTRODUCTION

IV.1.1-- Background

Doped metal oxides are systems of a host metal oxide (e.g. CaO, Y_2O_3) with a low-concentration of dopant (e.g. transition metals) incorporated into the host structure. The doped substance, therefore, often exhibits different properties from the host material, and unique applications may be possible only in the doped system. The europium-doped metal oxides that we investigated, for example, are efficient fluorescent materials and may be used as phosphors for flat panel displays or similar devices.

IV.1.2-- Goals

The doped metal oxide systems are significantly more complex than the monoelemental metal foils. Most importantly, the oxide samples test the ability to produce and identify unknown ions with our instrument. The low concentration of the dopant (5% and 0.033% for the Eu:Y_2O_3 and Eu:CaO, respectively) addresses the sensitivity of our LI-TOF-MS procedure. Although the theoretical composition of the metal oxides is known, these complicated solid samples challenge our mass calibration over a wider range. Upon successful ion identification, insight into some of the gas-phase reactions of these systems will be proposed. Furthermore, experimental isotopic abundance data for a variety of species will be compared to the natural abundances.

IV.1.3-- Samples investigated

Two different samples, both prepared by solid-state sintering, were analyzed with our TOF-MS. Initial investigations were performed with a sample of yttrium oxide doped with 5% europium (5% Eu:Y_2O_3), and subsequent studies were conducted on a 0.033% europium-doped calcium oxide (0.033%Eu:CaO) sample. These samples allowed both the study of different host materials and dopant concentrations.

For each sample, a 2-mm thick, 0.5-cm diameter pellet was ablated in the LI-TOF-MS. Methods of sample preparation to obtain each pellet differed, however. For the 5% Eu:Y_2O_3 sample, a dry mix procedure was employed. Appropriate ratios of yttrium oxide and europium powders were mixed thoroughly in a dry mill. The mixture

was then pressed into a 2-mm thick pellet in the die press and sintered in a crucible at ~1000°C to achieve homogeneity. The resulting pellet was inserted into the mass spectrometer on a sample holder attached to the sample probe. The 0.033% Eu:CaO sample was prepared by first dissolving europium oxide in dilute nitric acid. An appropriate amount of calcium oxide was then mixed into the solution and evaporated to form a powder. The powder was then pressed into a 2-mm thick pellet in the die press and sintered in a crucible at ~1000°C.

IV.2-- 5% Eu:Y_2O_3 results

Although the dopant concentration of this sample is not at trace analytical levels, generating and detecting europium ions tests the applicability of our LI-TOF-MS as an analytical tool. Laser ablation of the pellet was straightforward, with a 25-cm focal length lens creating an ~11 μm laser spot radius on the sample pellet. Significant signal improvements were achieved by ablating a fresh sample surface to prevent laser beam defocusing and by averaging up to 50 laser shots per spectrum. After initial experimentation, the optimum repeller delay times for the various masses were determined, as discussed in chapter III. Operating at delays intermediate between the optimum for the major sample ions generated a complete spectrum over a wider mass range (~50-500 amu). The delay time was also varied to search for higher-molecular mass species and prevent any instrumental bias and limiting of the data from improper repeller delay settings.

Table IV.1 highlights the major ions which were observed following laser ablation of the pellet, with an approximate (non-quantitative) intensity. As Figure IV.1 portrays, the most prominent species correspond to the bare metals (Y^+ and Eu^+) and their 1:1 metal:oxygen clusters (YO^+ and EuO^+). These ions dominated the yield regardless of the laser energies used (~10-40 μJ). Clearly, there was no problem detecting the europium dopant at this 5% concentration level. Also, a clean separation of both of the series of isotopes ($^{151}Eu^+$ and $^{153}Eu^+$, and $^{151}EuO^+$ and $^{153}EuO^+$) was obtained. After specific optimization for the europium ions, resolution in typical spectra was at least 400.

In addition to the main species in Table IV.1, minor components could be observed (See Table IV.2). Since the mass spectrometer samples the gas-phase products

Table IV. 1: Major ions observed for the ablation of the 5% Eu:Y_2O_3 pellet.

MASS (amu)	SPECIES	INTENSITY (1-10)
89	Y^+	10
96	YO^+	10
151, 153	Eu^+ isotopes	6
167, 169	EuO^+ isotopes	4

Table IV. 2: Minor components detected for high-energy ablation of the 5% Eu:Y_2O_3 pellet.

M/Z	SPECIES	PROBABLE ORIGIN
~44.45	Y^{2+}	Second ionization of yttrium
16	O^+	Ablated fragment
~210	$Y_2O_2^+$	Gas-phase aggregate

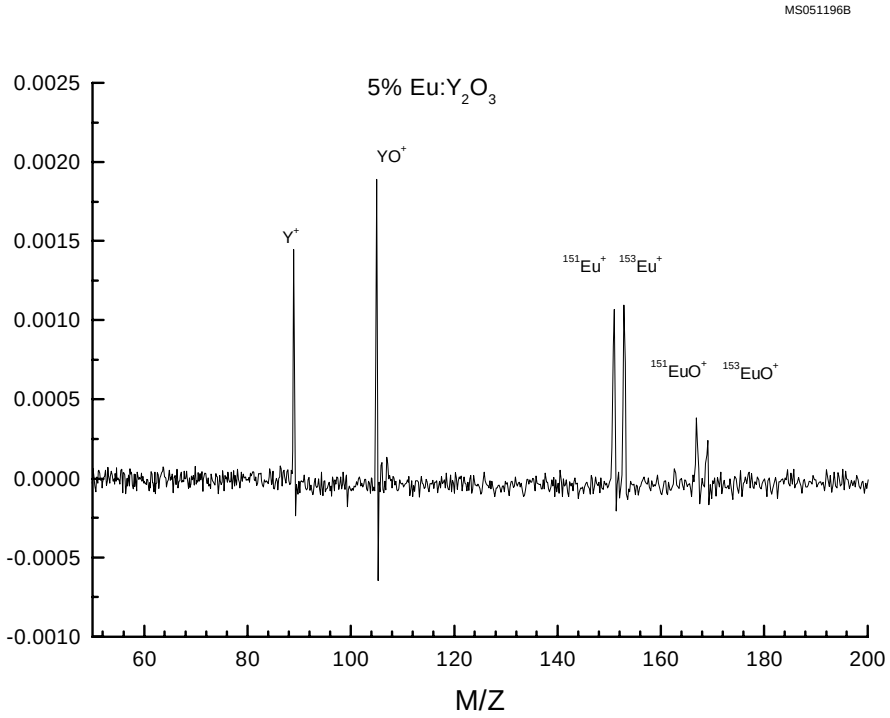

Figure IV. 1: Typical mass spectrum of the 5% Eu:Y_2O_3 sample.

of the laser-induced microplasma, gas-phase clusters, fragments, and aggregates are detected. The largest aggregate, $Y_2O_2^+$, was observed with a S/N ratio of ~2 on an inconsistent basis. Even when the laser energy was increased and long repeller delays (over ~25 μs) were employed to search for these aggregate products, the ion yield of $Y_2O_2^+$ accounted for less than a 10% relative yield to the nearest-mass ion, EuO^+. Furthermore, high-energy ablation produced bare oxygen ions, O^+, and doubly-charged yttrium, Y^{2+}. The small signals from these peaks, however, were observed on an inconsistent basis. Considering the high ionization energy of Y^{2+} (12.24 eV) it is not surprising that the ion yields were low and that this species was only detected using high laser energies. In addition, a relatively large oxygen atom content would be expected in the microplasma, but ionizing the oxygen to O^+ and detecting this species might be difficult. The high ionization energy (13.618 eV) and electron affinity (1.466 eV) favor the atomic species or negative ion over the positively charged ion.

IV.3-- 0.033% Eu:CaO results

Following the successful mass spectra of a 5% doped sample, a lower dopant concentration and different host were investigated. The 0.033% Eu:CaO pellet was ablated with similar conditions as the 5% Eu:Y_2O_3 (25-cm focal length lens, ~11 μm beam spot radius). Rotating the sample probe to ablate a fresh spot again improved the signal intensity and averaging 50 laser shots per spectrum increased the S/N ratio. Our TOF-MS experiments achieved resolutions between 400 and 500 for most of the ion peaks. A more systematic relation between the ablation energy and ion yield was studied, and increased emphasis was placed on the gas-phase aggregation products produced in the laser-induced microplasma.

IV.3.1-- Ion peak detection and identification

The primary objective of assuring instrument sensitivity was achieved, as europium-containing species provided significant ion peaks in the mass spectra. In contrast to the yttrium oxide material, the Eu:CaO sample yielded much more complex spectra, as is clear from Figure IV.2. Mass identification was therefore more difficult, but after calibration, the m/z values were related to major sample components such as

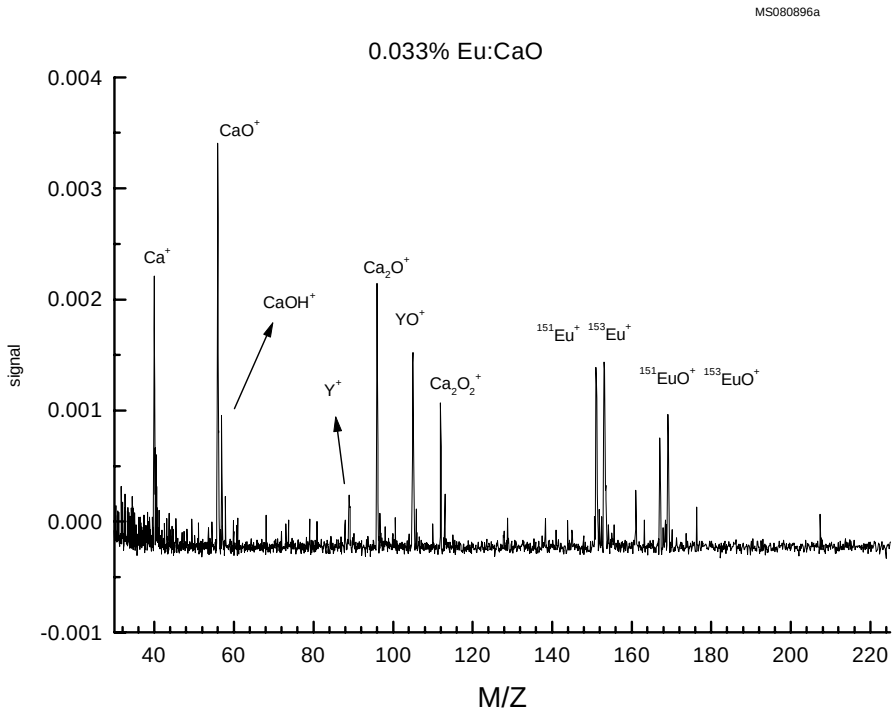

Figure IV. 2: Typical mass spectrum of the 0.033% Eu:CaO sample (TOF-MS conditions optimized for 100-200 amu mass range).

CaO^+ and gas-phase clusters. Mass accuracies, typically 0.1% or greater, aided in ion identification.

The most abundant ions in the majority of the mass spectra are listed in Table IV.3 with a corresponding approximate intensity. As with the Eu:Y_2O_3 sample, the bare metal ions of the Eu:CaO pellet (Ca^+ and Eu^+) and their corresponding oxides (CaO^+ and EuO^+) dominate the spectra. With the Eu:CaO sample, though, many more cluster ions such as Ca_2O^+ and $Ca_2O_2^+$ were observed. The intensities of the Ca_2O^+ and $Ca_2O_2^+$ clusters varied based on the extraction conditions (repeller delay), but in general had yields between 30% and 50% of the CaO peak. Other cluster ion peaks, as listed in Table IV.4, were observed with far less consistency and abundance. In general, a 1:1 ratio of Ca:O in the clusters was observed. Also, as with the 5% Eu:Y_2O_3 pellet, bare oxygen ions were produced at high laser energies (over ~50μJ).

Table IV. 3 : Major ions observed following ablation of the 0.033% Eu:CaO pellet.

MASS (amu)	SPECIES	INTENSITY (1-10)
40, 44	Ca^+ isotopes	10
56	CaO^+	9
96	Ca_2O^+	7
112	$Ca_2O_2^+$	7
151, 153	Eu^+ isotopes	6
167, 169	EuO^+ isotopes	4

Table IV. 4: Aggregation products detected for high-energy ablation of the 0.033% Eu:CaO pellet.

MASS (amu)	PROBABLE CLUSTER
~168	$Ca_3O_3^+$
~207, 209	$EuCaO^+$
~224	$Ca_4O_4^+$
~279, 281	$EuCa_2O_3^+$
~336	$Ca_6O_6^+$

IV.3.2-- Valence model explanation of observed gas-phase cluster ions

Referring to the "valence model" of oxide ion formation following laser radiation described by Stolyarova and Semenov[58], the "fragment valence", K, of a cluster $(M_nO_m)^{\pm}$ is expected to equal the group number of the metal,

$$K = \frac{q + 2m}{n}$$

Equation IV. 1 : Fragment valence for expected metal:oxygen ratios in main group metal oxide clusters.

where q is the charge of the cluster, and n and m are the number of metal and oxygen atoms, respectively.

Equation IV.1, applicable only to main group elements, indicates that the most common laser-produced clusters of $Ca_nO_m^+$ would have K ~ 2 since calcium is a group II metal. Ca_2O^+ (K=1.50), $Ca_2O_2^+$ (K=2.50), $Ca_3O_3^+$ (K= 2.33) and $Ca_4O_4^+$ (K= 2.25) are therefore more likely aggregates than other n:m ratios. Although only observed occasionally, the experimental identification of $Ca_2O_2^+$, $Ca_3O_3^+$, $Ca_4O_4^+$, and $Ca_6O_6^+$ as opposed to other ratios, confirms this theory. In addition to the calcium-oxygen clusters, small amounts of aggregates containing both Eu and Ca were detected. Table IV.4 summarizes the higher-mass gas-phase aggregates.

IV.3.3-- Analytical capabilities

The LI-TOF-MS investigation of the 0.033% Eu:CaO proved successful in determining contamination and hydration of the pellet. The detection of $CaOH^+$, Ca_2OH^+, and $Ca_2O_2H^+$ (~10%-25% abundance relative to the unhydrated species) reveal unexpected hydration of the sample. Hydration of the CaO pellet is not surprising due to the highly hygroscopic nature of CaO. It is also curious to note the peaks at m/z values of 89 amu and 105 amu. Comparing a Eu:Y_2O_3 spectrum (See Figure IV.1) with a Eu:CaO spectrum (See Figure IV.2), these peaks probably arise from contamination of the Eu:CaO pellet to provide Y^+ and YO^+ ions in the Eu:CaO spectra. Although the

[58] V. L. Stolyarova, G. A. Semenov, in J. FRS, Ed. *Mass Spectrometric Study of the Vaporization of Oxide Systems*. New York: John Wiley and Sons, 1994.

crucible was cleaned after each sintering, there may have been some Y_2O_3 residue in the crucible or the pellet press to contaminate the Eu:CaO pellet. Our LI-TOF-MS, therefore, successfully identified both unexpected hydration as well as contamination of this sample.

IV.3.4-- Dependence of spectra on laser energy

The relation between the laser energy and ion intensities was also studied. Threshold laser energies (~15 μJ) produced relatively abundant Ca^+, CaO^+, and Ca_2O^+ (S/N ratios each above 10), Eu^+ (S/N ~5), and a small amounts of $Ca_2O_2^+$, YO^+ and EuO^+ (S/N ~3). In general, these ion peaks intensified as the laser power was increased, but little of the higher-mass aggregates were observed until energy levels were increased to over ~40 μJ. The high-energy spectra also decreased the CaO^+ and EuO^+ yields relative to the bare ions Ca^+ and Eu^+. Because of the low yields of EuO^+, quantitative ratio data could not be obtained; however, an approximate 3:2 ratio of Eu^+:EuO^+ at threshold laser energies increased to about a 5:1 ratio of Eu^+:EuO^+ for ablation energies over ~40 μJ.

The intense Ca^+ and CaO^+ yields enabled quantitative studies of the dissociation of CaO^+ as a function of laser energy. Three energies were investigated thoroughly, ~18 μJ, 22 μJ, and 25 μJ, and both peak height and area data were gathered. The mean Ca^+/CaO^+ ratio for ten spectra, each compiled by averaging 50 laser shots, is highlighted in Table IV.5.

Table IV. 5 : Relative yield of Ca^+/CaO^+ as a function of laser energy.

LASER ENERGY (μJ)		**RATIO Ca^+/CaO^+**	
		PEAK HEIGHTS	**PEAK AREAS**
18	**MEAN**	1.17	2.80
	%RSD	5.77%	11.70%
22	**MEAN**	3.15	9.68
	%RSD	17.57%	9.57%
25	**MEAN**	3.89	14.38
	%RSD	17.34%	5.41%

The yield of Ca^+ relative to CaO^+ clearly increases as the laser energy is increased. Both peak height and peak area data reveal the same trend, although the magnitude of the area data more thoroughly portrays the increased dissociation of the CaO^+ as a function of the ablation energy. Analyzing the area data, the Ca^+ yield relative to CaO^+ increases from 2.80 for ablation energies of 18μJ, to 9.67 with 22 μJ laser energies, to 14.39 as the laser energy is incremented to 25 μJ. The proportion thus is over 500% greater for the highest laser energy (25 μJ). With the peak height data, the ratio of Ca^+/CaO^+ is less than the peak area results. The proportion increases by approximately 350% from 1.17 to 3.89 for the lowest and highest ablation energies. Relative standard deviations decrease as the ratio increases for the peak area data, whereas the %RSD values increase from under 6% to over 17% for peak height data. One explanation of the significant decrease in the CaO^+ yield, as with the EuO^+ yield, is the fragmentation of the oxide to the bare metal ion. In addition, the greater ion density in the more energetic microplasma seems to promote aggregation to form larger clusters.

IV.4-- ISOTOPE ANALYSIS

IV.4.1-- Importance

Another important aspect of analyzing relatively simple systems such as the pure metal foils and doped metal oxides is producing mass spectra that reflect the known isotopic abundances of the species. Of highest priority for our initial studies, it is a crucial diagnostic tool for proper instrument characterization and optimization because mass resolution, linearity of peak areas, and accurate data analyses are required. Therefore, one test of the new instrument is to analyze these simple systems to prove the ability of our LI-TOF-MS to make fundamental measurements and calculations. Furthermore, once it is determined that the isotopic abundances portrayed are indeed reliable, complex mixtures may be characterized with greater confidence; the masses calculated from the times of flight of the ions can be confirmed by comparing the isotopic distributions with the known values. This may also allow the identification of isobaric

interferences, since one mass of the isotope distribution will be uncharacteristically too intense.

Calculations of the relative abundances are possible since the area under each mass spectral peak is directly related to the ion yield. Although calculations based on peak heights are much simpler and often provide useful approximations, truly quantitative results need to be based on the integrated area beneath the peak. For this to be possible, baseline mass resolution of each isotope must be achieved. We may take the example of the tungsten isotopes of 182, 183, 184, and 186 amu to see that a resolution ($m/\Delta m$) of approximately 200 or greater is required. This was indeed achieved experimentally, as Figure IV.3 reveals. Furthermore, higher resolutions and enhanced separations lead to easier quantitation and integration.

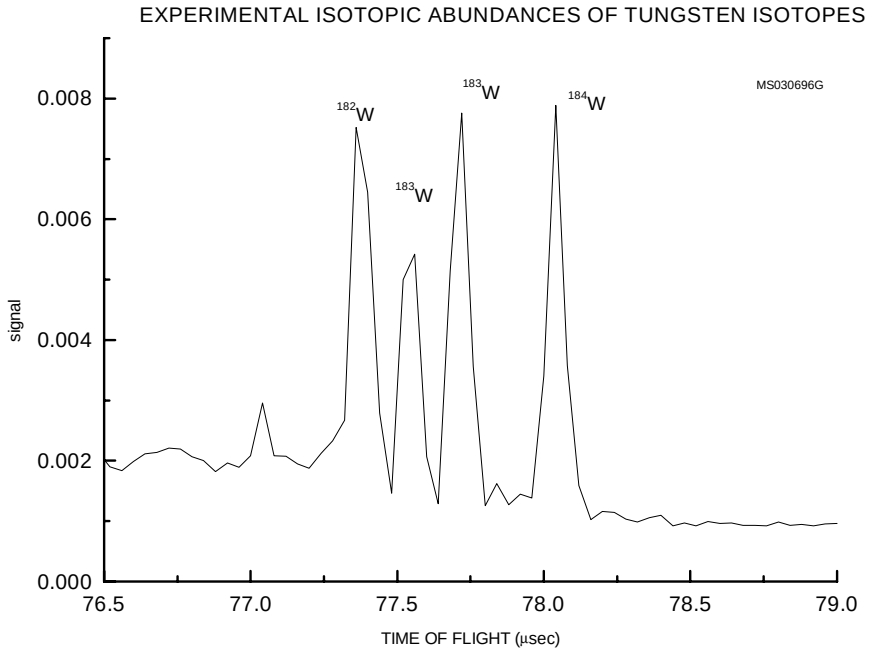

Figure IV. 3: Mass spectral resolution and quantitation of tungsten isotopes.

IV.4.2-- Results and Conclusions

The data in Table IV.6 show that for both the pure metal foils (tungsten, indium) and ions from the doped oxides (europium and europium oxide, calcium), the most accurate results were obtained when the relative natural abundances are similar to each other. This is clear by analyzing the tungsten and europium data in the table. Looking at the tungsten experimental data, the calculated distribution is over 97% accurate for the masses with similar abundances [^{182}W (26.31% relative abundance), ^{184}W (30.64%), and ^{186}W (28.64%)]. Similarly, successful results were obtained with the europium species as accuracies of greater than 99% were achieved for the bare europium ion [^{151}Eu (47.77% relative occurrence), ^{153}Eu(52.22%)]. In addition, experimental calculations of the EuO peaks of the 0.033% Eu:CaO showed success of over 98.5% for both the ^{151}EuO and ^{153}EuO isotopes.

Unfortunately, in cases where there is a large difference between the natural abundances of the isotopes of a given element, the experimental data did not reflect the known isotopic abundance values. Taking the worst-case scenario of ^{44}Ca, our results revealed an 8.58% relative abundance experimentally compared to a known relative abundance of only 2.13%. In much the same manner, the mean experimental abundance of the ^{113}In (14.71%) was much greater than the known abundance of 4.16%.

Several sources of error could account for the discrepancies between the experimental and known data of the lower-abundance isotopes. Most significant are limitations in the ion recording system and dynamic range of the ion detector[59]. Odom and Schueler found similar problems in their LIMS studies[60], and as they rightly reveal, a detector dynamic range of over 20:1 is needed for accurate ^{113}In/^{115}In investigations. Therefore, the excessively high signal of the less abundant species might be attributed to the saturation of the more intense peak to improve the S/N ratio of the lesser isotope. Integrations are thus accurate for the less-abundant mass, but inaccurately low for the more-abundant isotope and overall ion yield of the species. For example, saturation

[59]I. Koumenis, M. Vestal, A. Yergey, S. Abrams, S. Derring, T. Hutchers. *Anal. Chem.* **67** (1995) 4557.

[60] R. Odom, B. Schueler, in Chap. 5, D. Lubman, Ed. *Lasers and Mass Spectrometry*. Oxford University Press, 1990.

Table IV. 6 : Isotopic abundance results.

TUNGSTEN ISOTOPE DATA	**Sample: Pure tungsten foil**				
	W^+ isotope mass	182	183	184	186
	Natural abundance (%)	26.31	14.28	30.64	28.64
	Experimental determination:				
	Relative abundance (%)	25.57	17.57	29.73	27.95
	Std Dev.	3.625	1.804	1.479	1.475
	DIFFERENCE FROM KNOWN NATURAL ABUNDANCE	2.83%	23.02%	2.98%	2.40%
INDIUM ISOTOPE DATA	**Sample: Pure indium foil**				
	In^+ isotope mass	113		115	
	Natural abundance (%)	4.16		96.84	
	Experimental determination:				
	Relative abundance (%)	14.71		85.29	
	Std Dev.	2.131		2.131	
	DIFFERENCE FROM KNOWN NATURAL ABUNDANCE	253.65%		11.01%	

Table IV. 6(continued) : Isotopic abundance results.

CALCIUM ISOTOPE DATA	**SAMPLE: 0.033% Eu:CaO**		
	Ca^+ isotope mass	40	44
	Natural abundance (%)	96.92	2.13
	Experimental determination:		
	Relative abundance (%)	91.42	8.58
	Std Dev.	0.55	0.55
	DIFFERENCE FROM KNOWN NATURAL ABUNDANCE	5.67%	302.81%
EUROPIUM ISOTOPE DATA	**SAMPLE: 0.033% Eu: CaO**		
	Eu^+ isotope mass	151	153
	Natural abundance (%)	47.77	52.22
	Experimental determination:		
	Relative abundance (%)	47.37	52.63
	Std Dev.	0.83	0.78
	DIFFERENCE FROM KNOWN NATURAL ABUNDANCE	0.83%	0.78%
EUROPIUM OXIDE ISOTOPE DATA	**SAMPLE: 0.033% Eu: CaO**		
	EuO^+ isotope mass	167	169
	Species	$^{151}Eu^{16}O$	$^{151}Eu^{18}O$ and $^{153}Eu^{16}O$
	Natural abundance (%)	47.30	52.68
	Experimental determination:		
	Relative abundance (%)	47.94	52.07
	Std Dev.	1.79	1.79
	DIFFERENCE FROM KNOWN NATURAL ABUNDANCE	1.35%	1.16%

effects in the indium data would be revealed in an inaccurately high ^{113}In relative percentage, as was observed. Another possible complication is the over-integration of noise associated with the measurement. This could affect the less abundant isotope quite significantly by increasing the ion yield calculation. Finally, a more subtle complication may arise from limitations in the voltage digitization of the oscilloscope[60].

Other notes are important to discuss regarding the observed data. The ^{42}Ca isotope (0.64% relative abundance) was unable to be consistently integrated within the dynamic range limitations of the detector and the noise level of the measurements, and it was thus omitted from the data table. The oxygen isotope ^{18}O, which accounts for only 2.04% of the known oxygen abundance, was not reliably integrated by itself and also omitted from the data table. However, since this isotope should account for a small but present amount of signal, it was added into the known isotopic calculations for the oxide-containing ^{151}Eu^{18}O (169 amu).